Phason dispersion in the incommensurate phase of betaine calcium chloride dihydrate

1997 J. Phys.: Condens. Matter 9 1461

(http://iopscience.iop.org/0953-8984/9/7/011)

J. Phys.: Condens. Matter **9** (1997) 1461–1475. Printed in the UK PII: S0953-8984(97)75527-9

Phason dispersion in the incommensurate phase of betaine calcium chloride dihydrate

J Hlinka†§, M Quilichini†, R Currat‡ and J F Legrand‡

† Laboratoire Léon Brillouin, CEA de Saclay, Gif-sur-Yvette, France

‡ Institute Laue–Langevin, 38042 Grenoble, France

Received 18 June 1996, in final form 7 October 1996

Abstract. The phonon excitations derived from the three lowest-frequency Λ_3–Λ_2 extended branches in the incommensurate phase of betaine calcium chloride dihydrate (BCCD) are studied at 145 K by coherent inelastic neutron scattering. For the first time the amplitudon–phason splitting is observed in the entire extended Brillouin zone. A phenomenological mode coupling approach is suggested, which provides a description of the observed spectra beyond the usual limiting case $T \to T_i$.

1. Introduction

In the large family of known structurally incommensurate dielectric crystals [1], betaine calcium (di)chloride dihydrate (BCCD: $(CH_3)_3NCH_2COO \cdot CaCl_2 \cdot 2H_2O$) is the compound with the largest number of commensurate modulated phases. Most of the experimental and theoretical studies of the 'devil's-staircase-like' phase diagram of this system were reviewed in [2] and [3]. At ambient conditions, BCCD is in its normal, nonmodulated high-temperature phase with orthorhombic *Pnma* symmetry and four formula units per unit cell [4]. At atmospheric pressure the modulation appears below $T_i = 165$ K, with the incommensurate modulation wavevector $q_s \approx 0.33c^*$ decreasing continuously with decreasing temperature. Most of the known commensurate phases appear below 127 K (table 1). The structure and superspace symmetry group ($P(Pnma)$:$(1, s, -1)$) of the incommensurate phase (INC-phase) were determined according to the x-ray data collected at 130 K [5]. The incommensurate phase can be viewed as the normal phase (N-phase) *Pnma* structure distorted by the condensation of the normal mode of Λ_3 symmetry (antisymmetric with respect to the mirror plane m and symmetric with respect to the glide plane a). A soft mode belonging to this representation was observed in the N-phase of BCCD in an inelastic neutron scattering experiment [6]. Recently, the dispersion of the four extended Λ_3–Λ_2 branches was investigated in detail in fully deuterated BCCD by inelastic neutron scattering [7] and a semi-microscopic model describing the mechanism of the transition into the INC-phase was proposed [8]. The present study is focused on the low-frequency excitations of the incommensurate phase, derived from the extended Λ_3–Λ_2 branches of the normal phase.

The lattice dynamics of incommensurate displacive dielectrics has been studied by inelastic neutron scattering since 1980 [9–12]. The so-called phason branch, corresponding

§ Present address: Institute of Physics AV CR, Na Slovance 2, 1890 40 Praha 8, Czech Republic. e-mail: hlinka@fzu.cz

0953-8984/97/071461+15$19.50

Table 1. The phase diagram of BCCD: domains of stability of the principal modulated phases, at normal pressure.

q_s/c^*	Range of stability (K)
INC 1	128–165
2/7	125–127
INC 2	115–128
1/4	76–115
1/5	53–75
1/6	47–53
0	–46

to fluctuations of the phase of the incommensurate modulation, attracted most of the attention. As the potential is invariant with respect to an arbitrary translation of the modulation in the incommensurate phase, the frequency of the uniform phase mode vanishes. In the long-wavelength limit the dispersion of the phason branch is linear, similar to the dispersion of the acoustic branches. Inelastic neutron scattering is the only technique able to unambiguously detect the phason branch. It has been observed in four systems so far: biphenyl [9], K_2SeO_4 [10], $ThBr_4$ [11] and most recently BCPS [13]. Experimentally, the distinction between acoustic and phason branches is based on differences in their slopes, as in biphenyl [9], or scattering intensities, as in $ThBr_4$ [11], or in their damping constants, as in K_2SeO_4 [10].

Another characteristic excitation of the modulated phase is the so called amplitudon mode, the frequency of which vanishes at the phase transition but which renormalizes below T_i as an ordinary soft mode. It was observed in $ThBr_4$ [11] and biphenyl by inelastic neutron scattering and in many other systems by Raman spectroscopy. This mode was introduced by Axe [14] in the frame of a simple phenomenological Landau model for a sinusoidal modulation. It corresponds to fluctuations of the amplitude of the modulation.

In comparison with the four previously studied systems BCCD differs considerably in the character of its phase diagram. In three of the four above-mentioned systems, where at least part of the phason branch was seen as an *underdamped* excitation ($ThBr_4$, biphenyl and BCPS), the temperature dependence of the modulation wavevector is quite limited and the modulation apparently remains incommensurate down to very low temperature. For K_2SeO_4, where the phason was observed as an *overdamped* excitation, a lock-in transition into a commensurate 1/3 phase occurs near 90 K. In the case of BCCD the modulation wavevector shows a remarkable temperature dependence and the incommensurate phase is followed by a large number of commensurate phases, on cooling.

BCCD differs also from the other systems studied so far in the complexity of the low-frequency Raman and infrared results observed in the incommensurate phase and in the ambiguities which have occurred in their interpretation [15–18].

Recently, a qualitative model for several low-energy branches in the incommensurate phase was published, based on available far-infrared and Raman data at 145 K [18]. In this model, the dispersion curves are assumed to have almost the same dispersions as in the N-phase, because all expected splittings are considered negligible with the exception of the amplitudon–phason splitting. The present experimental data do not confirm the simple picture proposed in [18], in spite of the fact that our data were taken at 145 K, i.e. only about 20 K below T_i. This temperature is comparable with the conditions under which the phason dispersion was measured in $ThBr_4$, biphenyl and K_2SeO_4 (15, 15 and 10 K below

T_i respectively), where the simple amplitudon–phason splitting was observed. We argue in the following that the failure of the simple amplitudon–phason splitting model can be ascribed to the fact that the soft branch has a rather weak dispersion in BCCD.

The article is organized as follows. The experimental details are given in the next section. In section 3 we present the experimentally determined dispersions of the excitations derived from the three lowest-frequency Λ_3–Λ_2 extended branches, as obtained by inelastic neutron scattering experiment on BCCD at 145 K. Section 4 is devoted to the analysis of the incommensurate phase excitations in the frame of a simple phenomenological model, and the required extensions of the traditional approach are introduced. Finally, in section 5 the present results are reviewed and discussed.

2. Experimental details

The present experiment was performed under the same experimental conditions and with the same sample as the previous study of the excitations in the N-phase [7].

The sample was an approximately 2 cm^3 single crystal of BCCD grown by slow evaporation from a saturated solution of totally deuterated chemicals by J M Godard (Laboratoire de Physique des Solides, Université Paris-Sud, Orsay). It is known that deuteration has almost negligible effects on the phase diagram of BCCD (see, for example, [19]), and it significantly reduces the incoherent neutron scattering signal from the hydrogen nuclei, which strongly perturb the coherent neutron scattering experiments.

The crystal, enclosed in an aluminium container, was mounted on the cold finger of a closed cycle refrigerator. The temperature stability was better than 0.05 K. All measurements were performed on the 4F1 and 4F2 three-axis spectrometers located on a cold source at the Orphée Reactor at CE Saclay (France). All scans were performed in the 'constant-k_i mode' (i.e. with fixed incident neutron wavevector k_i) and neutron energy gain. Both monochromator (vertically bent) and analyser (flat) crystals were pyrolitic graphite (PG[002]). A Be or PG filter was used on the incident beam to avoid second-order contamination. Horizontal collimations on incoming and scattered neutron beams were such that the instrumental energy resolution, measured on a vanadium sample, could be varied from $\Delta E = 0.25$ THz for $k_i = 2.662$ Å^{-1} to $\Delta E = 0.015$ THz for $k_i = 1.2$ Å^{-1}.

A systematic data analysis, accounting for the effect of instrumental resolution, was performed. For this purpose we used the set of standard LLB programs [20]. The resolution is modelled by a Gaussian function in four-dimensional ($\boldsymbol{Q}$, ω) space and it is calculated at each point of the scan independently. The experimental data are then fitted by the convolution of the parametrized differential cross-section with the resolution function. The principal contributions to the total cross-section are the elastic scattering from the main and satellite reflections, the elastic incoherent scattering and the inelastic coherent cross-section.

Special attention was paid to possible parasitic scattering contributions due to the finite resolution. The elastic incoherent scattering was measured at several points of the Brillouin zone and then kept fixed in all fits in a given Brillouin zone in the same way as for the inelastic background.

The inelastic phonon cross-section was taken in the form of the response from independent damped oscillators:

$$S(\boldsymbol{Q}, \omega) = \sum_{\nu=1}^{all\ modes} S_\nu(\boldsymbol{Q}, \omega) \tag{1}$$

where the summation is over all vibrational modes of the crystal, expected to contribute in

the examined frequency range, and where

$$S_\nu(\boldsymbol{Q},\,\omega) = \langle n(\omega)\rangle \left|F_{\nu,in}(\boldsymbol{Q})\right|^2 R_\nu(\omega)\delta(\boldsymbol{Q}\pm\boldsymbol{q}-\boldsymbol{G}) \tag{2}$$

is the scattering function of a single phonon branch ν.

In this expression $\langle n(\omega)\rangle$ is the Bose–Einstein distribution, $R_\nu(\omega)$ is the response function of a single damped harmonic oscillator,

$$R_\nu(\omega) = \mathrm{Im}\left\{\frac{1}{\omega_\nu^2 - \mathrm{i}\gamma\omega - \omega^2}\right\} = \frac{\omega\Gamma_\nu(\boldsymbol{q},\,T)}{(\omega^2-\omega_\nu^2(\boldsymbol{q},\,T))^2+\omega^2\Gamma_\nu^2(\boldsymbol{q},\,T)} \tag{3}$$

and the multiplicative constant $|F_{in}(\boldsymbol{Q})|^2$ is the square of the inelastic structure factor. In the normal periodic crystal it is given by

$$F_{\nu,in}(\boldsymbol{Q}) = \sum_{j=1}^{unit\ \ cell} m_j^{-1/2} b_j \left[\boldsymbol{e}_j^\nu(\boldsymbol{q})\cdot\boldsymbol{Q}\right]\exp\left(\mathrm{i}\boldsymbol{Q}\cdot\boldsymbol{r}_j\right)\exp\left(-W_j(Q)\right) \tag{4}$$

where m_j is the mass of atom j, b_j its coherent scattering length, $W_j(Q)$ is the exponent of the Debye–Waller factor and $\boldsymbol{e}_j^\nu$ is the eigenvector of the νth mode. The inelastic structure factor in the incommensurate crystal can be written in the same form if the unit cell is assumed to be infinite in the direction of modulation.

In order to take full advantage of the continuity of the transition to the modulated phase, we worked in the same extended zone scheme as in the parent N-phase. More precisely, excitations observed for a total momentum transfer vector $\boldsymbol{Q}$ in the (b^*c^*) plane are labelled by a wavevector $\boldsymbol{q}$ defined as the smallest vector fulfilling $\boldsymbol{Q}=\boldsymbol{G}+\boldsymbol{q}$, where $\boldsymbol{G}$ corresponds to a non-extinct main Bragg peak ($k+l$ even).

The results presented below were obtained from measurements performed mostly in the (0 2 q), (0 4 q) and (0 3 $3\pm q$) extended Brillouin zones, as for the N-phase experiment in [7]. Measurements in these zones are mutually complementary, in the sense that each zone is the most convenient one for studying a particular phonon branch.

3. Experimental results

The present experiment was performed at 145 K, that is, roughly 20 K below T_i. At this temperature, the modulation can be still considered as quasi-sinusoidal, because all higher-order satellites are of very low intensity. The most pronounced higher-order satellites have intensities more than two orders of magnitude lower than the first-order satellites.

The interpretation of the inelastic scattering data in the incommensurate phase was to a large extent facilitated by the comparison with previous data in the N-phase [7]. In the N-phase the dispersion can be viewed as resulting from the anticrossing of the two rather flat optic branches B_{2u}–A_u and B_{3g}–B_{1g}, with the extended bare acoustic branch with a $\sin(\pi q/2)$-like dispersion (figure 1). From these measurements we learnt that the higher bare optic branch, at roughly 0.6 THz, has a large structure factor in the (0 3 0) zone, while the lower branch, around 0.3 THz, provides large intensity in the (0 4 0) extended zone.

The dispersion observed in the incommensurate phase can be approximately described in a similar manner. Again, we observed an anticrossing of the acoustic branch with the flat optic branch near 0.6 THz with strong intensity in the (0 3 3) extended Brillouin zone.

The interpretation of the spectra measured in the (0 4 q) extended zone requires us to consider at least the following three contributions:

(1) an underdamped mode around 0.4 THz;
(2) an overdamped mode;

(3) another underdamped mode, much more dispersive and visible only around the satellite peak (0 4 q_s).

By comparison with the dispersion of the transverse acoustic branch measured around the strong (0 2 0) Bragg peak, we have identified the dispersive branch as the transverse acoustic phonon branch originating from the satellite position (0 4 q_s).

The existence of the supplementary underdamped branch extending over the whole Brillouin zone is more surprising. Theoretically, one expects that close to T_i the soft-mode branch splits near q_s into a phason and an amplitudon branch [14, 21, 22]. As the phason frequency goes to zero at q_s, while its damping remains finite, it should have overdamped dynamics near q_s [23]. Therefore, we assume that the observed overdamped branch corresponds to the phason branch. However, unlike the case in the usual scheme, our measurements show that the lower soft optic branch is split into at least two components in the *whole* (extended) Brillouin zone. Indeed, even at the extended Brillouin zone boundary, we can observe the appearance of an additional mode below T_i (see figure 2). Using continuity, we can interpret the two lowest-frequency modes as 'split A_u sub-modes'. This clearly shows that the present results do not correspond to the regime usually discussed in the $T \rightarrow T_i$ limit. In the following we assume as a starting hypothesis that the phason–amplitudon splitting can be simply extended to the whole lower optic branch. The experimental data were than fitted systematically with the appropriate number of independent damped harmonic oscillators.

The fit of the overdamped mode does not allow us to determine the frequency and damping constant independently. We have thus measured the phason dispersion around (0 4 q_s) also in the 'hard' direction b^* (see figure 3). At (0 3.9 q_s) the phason frequency is sufficiently high to estimate the value of the damping coefficient at $\gamma \approx 0.3$ THz. This value was then imposed in all fitted spectra, which allowed us to obtain the dispersion of the phason branch displayed in figure 1. Roughly the same damping was found also for the optic branch near 0.4 THz, and this value was imposed during the fitting of some spectra also for this branch.

Several examples of experimental spectra with their interpretation are provided in (figures 4–6). Figure 4 shows the spectrum obtained at the zone centre point $\boldsymbol{Q} = (0\ 4\ 0)$ at 145 K. The large signal at zero frequency corresponds mainly to the (0 4 0) Bragg scattering. The contribution of the acoustic modes emanating from this Bragg reflection, that appears due to the finite instrumental resolution, is simulated by a Lorentzian function centred at zero frequency and adjusted using the experimental data in the N-phase [7]. As already mentioned, the damping constant of the lower, overdamped mode is fixed at 0.3 THz. In the same spectrum above T_i only the B_{2u} mode was seen. In this sense, the spectrum is equivalent to the infrared spectrum $E \parallel y$. The overdamped mode and the mode at 0.49 THz correspond thus to the 'splitting' of the B_{2u} mode. The same two components were observed in the infrared spectrum $E \parallel y$ [15, 18].

Figure 5 shows the spectrum at $\boldsymbol{Q} = (0\ 4\ 0.41)$ ($q = 0.41c^*$). The central part of the spectrum is fitted with three contributions: an overdamped phason mode, an elastic incoherent signal with resolution limited width and the acoustic mode emanating from the satellite at $\boldsymbol{Q} \approx (0\ 4\ 0.31)$ (the side peak at 0.15 THz). The damping constant of the phason and the intensity of the elastic incoherent contribution were obtained independently from spectra measured away from the c^*-direction. Phason, amplitudon and second optic branch, as measured at $\boldsymbol{Q} = (0\ 4\ 0.85)$, 20 K below T_i, are shown in figure 6.

Finally, attempts to observe directly the amplitudon at $q = q_s$ were unsuccessful. The main difficulty is caused by the very large signal from the overdamped phason. We

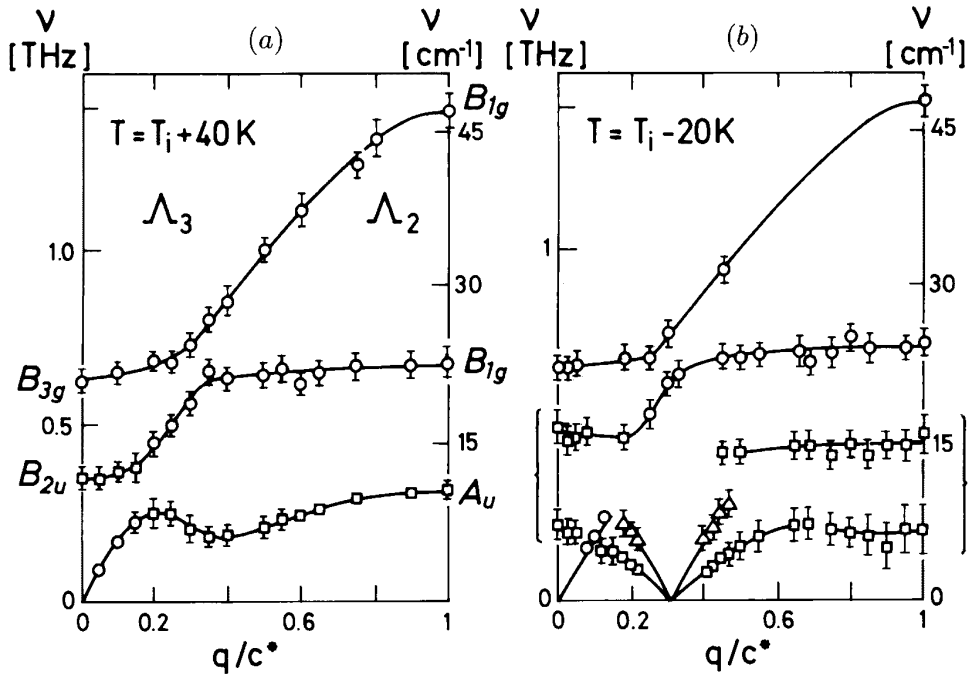

Figure 1. A comparison of the dispersion curves above and below T_i. The points were obtained from damped harmonic oscillator fits of the inelastic neutron scattering spectra; the full lines are guides for the eye. (*a*) Dispersion of the three lowest-frequency extended Λ_3–Λ_2 branches in the N-phase at 205 K (40 K above T_i [7]). (*b*) Dispersion in the INC-phase at 145 K (20 K below T_i). The comparison with the N-phase results, and the continuity of the structure factors, shows that the two lowest optic branches at 0.2 and 0.4 THz are derived from the lower bare optic branch observed in the N-phase. The lowest branch is identified as the 'phason branch'. The triangles correspond to the acoustic branch originating from the satellite reflection near $q_s = 0.305c^*$.

compared the damped harmonic oscillator responses of the two modes, one having a damping coefficient of 0.3 THz and very low frequency and the other having the same dynamical parameters as the lowest resolved peak in the Raman A_g spectra (i.e. frequency around 0.38 THz and damping about 0.24 THz [24]). We then argue that if the two modes have about the same structure factor, as expected, the amplitudon will give only a tiny contribution to the tail of the phason response, hardly detectable experimentally.

4. Excitations in the incommensurate phase

The excitations in the incommensurate phase may be expressed as normalized linear combinations of the modes of the normal phase [25]:

$$\eta_i = \sum_{q,j} \beta_{i;q,j}\eta_{q,j} \qquad \beta_{i;q,j} = \langle \eta_{q,j} | \eta_i \rangle \qquad \sum_i |\beta_{i;q,j}|^2 = 1 \tag{5}$$

where the summation may be over all modes in the direction of the modulation. The scattering cross-section for the new excitations is determined mainly by the following four facts.

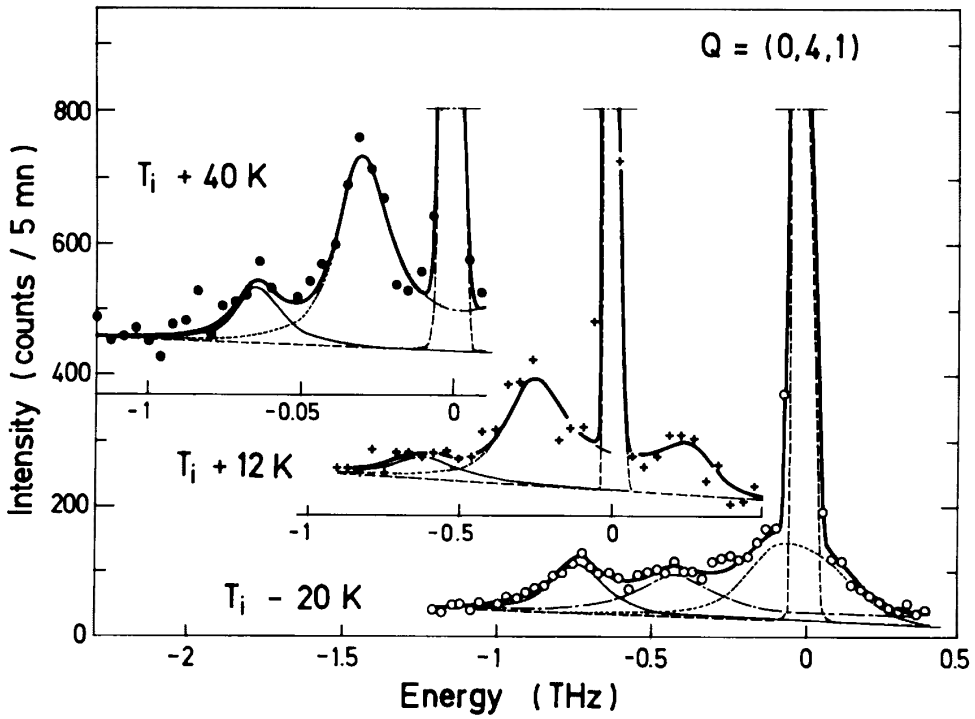

Figure 2. Experimental spectra corresponding to the momentum transfer vector $\boldsymbol{Q} = (0\ 4\ 1)$ at three temperatures. The full line is the convolution of the fitted response function with the instrumental resolution. Two modes are resolved in the N-phase spectra (40 and 12 K above T_i): the lower-frequency peak is the A_u mode, and the upper one is the Raman B_{1g} mode. These modes correspond to the (extended) zone boundary modes of the two flat optic Λ_3–Λ_2 branches shown in figure 1. Below T_i, three modes can be resolved.

(i) *The mean positions of the atoms in the incommensurate phase differ from those in the normal phase*. This implies that, as the order parameter grows, even the structure factor of the modes which have essentially the same eigenvector in both the INC- and N-phases may change.

(ii) *Due to the very low-frequency excitations (phason) the thermal fluctuations are large in the INC-phase*. This implies that the role of the Debye–Waller factor may be important. For details see [26] but also [27]; [28] but also [29] and [25].

(iii) *The eigenvectors of the new excitation contain contributions of the N-phase modes with different wavevectors q*. Therefore, the new excitations should be seen in all spectra (i.e. for all values of the momentum transfer vector $\boldsymbol{Q}$), where one of the contributing N-phase modes could be observed above T_i. Due to the linearity of the structure factor as a function of the eigenvector, the structure factor of the new excitation η_i is reduced with respect to the structure factor of the N-phase mode η_{qj} by the factor $\beta_{i;q,j}$, appearing in expression (5).

(iv) *The satellite peak may be considered a a new 'Brillouin zone centre'*. Consequently, even modes with eigenvectors that are essentially unperturbed by the phase transition may be observed at additional values of the total momentum transfer vector $\boldsymbol{Q}$. This is particularly

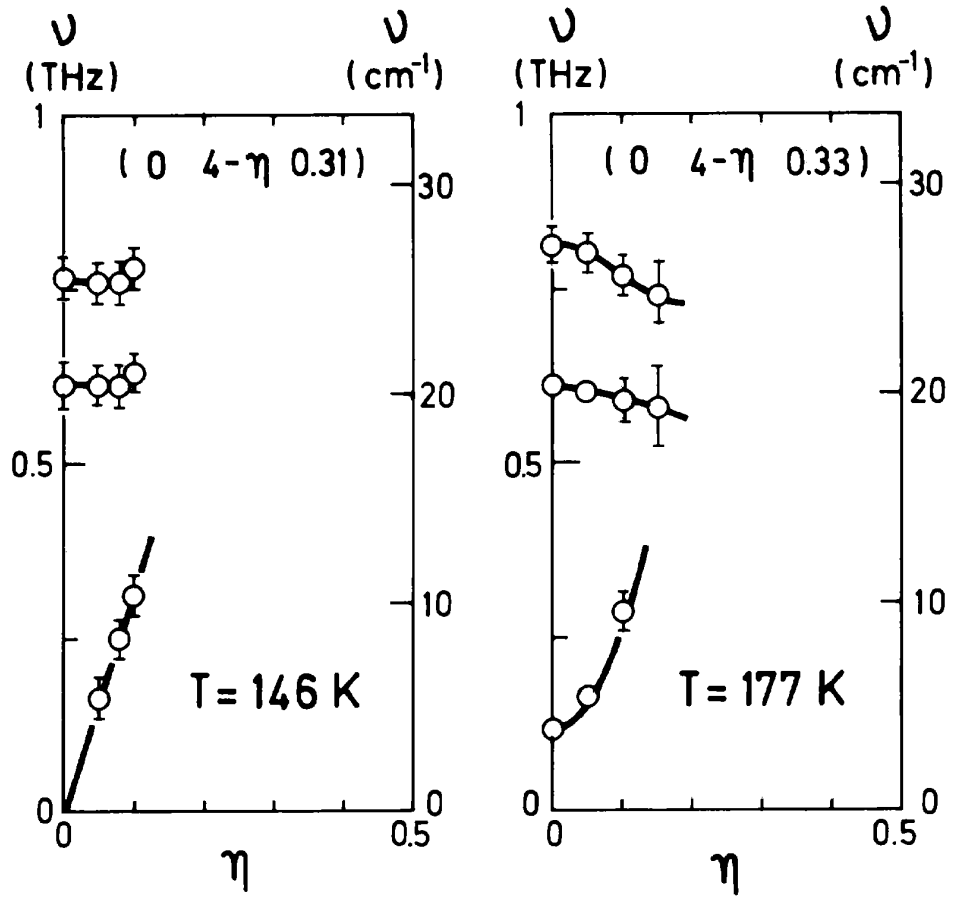

Figure 3. Dispersion of the phason branch 20 K below T_i (left) and of the soft mode 12 K above T_i (right) along the 'hard' direction b^*. Open circles are the results of the fits; continuous lines are guides for the eye. Spectra measured at wavevectors q with a nonzero component in the hard direction have been used to estimate the damping of the phason and the intensity of the elastic incoherent signal, which both vary smoothly with q.

true for the acoustic modes, which can be seen around the strong satellite peaks. This can be understood from the fact that the long-wavelength acoustic phonon structure factor differs from the elastic structure factor only by the multiplicative scalar product $(\boldsymbol{Q} \cdot \boldsymbol{u})$, where $\boldsymbol{u}$ is the acoustic mode polarization vector. Therefore, as long as this scalar product is nonzero, the intensity of the corresponding acoustic mode scales with the intensity of the Bragg reflection from which the acoustic dispersion originates. The explicit expressions for the general case are discussed in [30] and [35].

For the excitation originating from the soft branch, the third aspect, directly reflecting the mixing of the N-phase normal modes, is the most important one. It is usual to suppose that below T_i the soft branch, near q_s, is split into a 'phason' and an 'amplitudon' part, while the other modes remain more or less unchanged. This theoretical prediction is based on the following two principal assumptions about the additional couplings induced by the

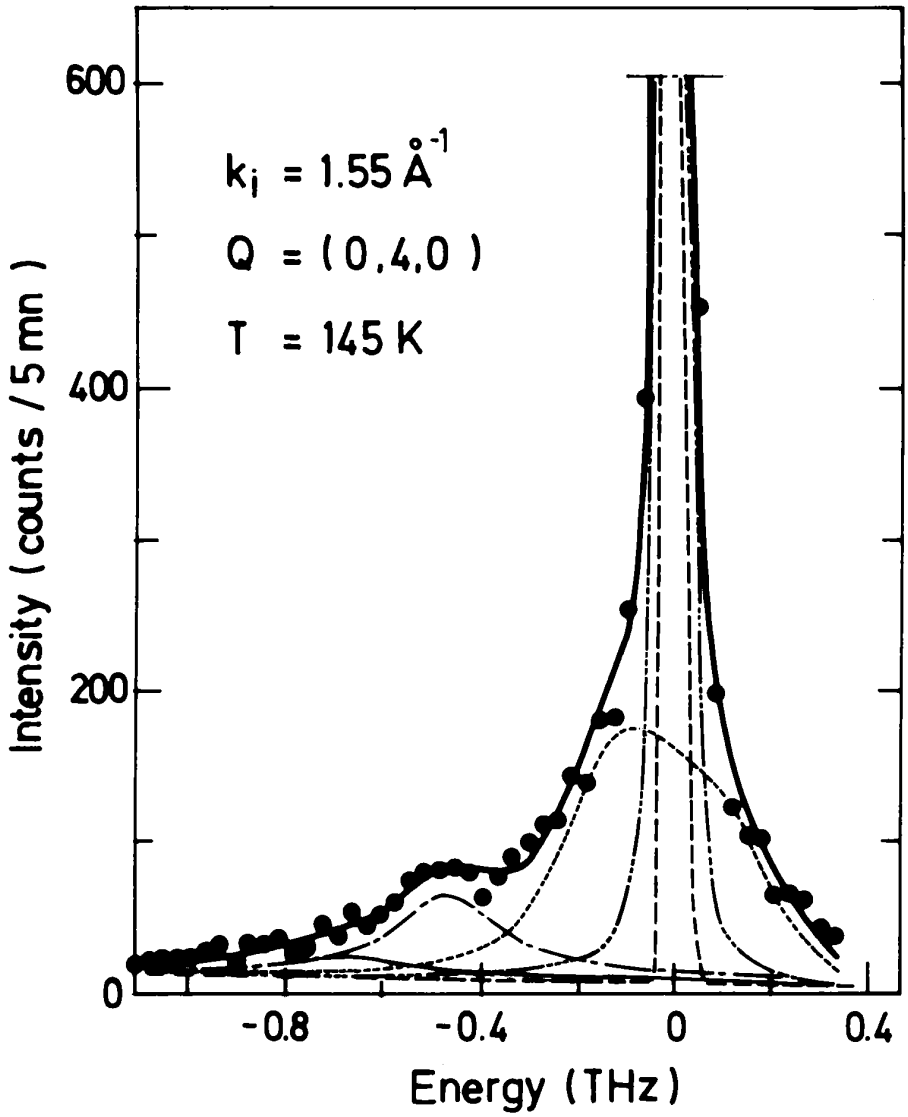

Figure 4. The experimental spectrum obtained at the zone centre point $\boldsymbol{Q} = (0\ 4\ 0)$ at 145 K. The dashed lines represent the different contributions included in the fit (full line).

frozen modulation wave:

(i) each normal mode of the soft branch $Q(q)$ is directly coupled only to the modes $Q(q + 2q_s)$ and $Q(q - 2q_s)$;

(ii) we can neglect all coupling terms except those between pairs of modes $Q(q)$, $Q(q - 2q_s)$, with $q \approx q_s$ (and $Q(q)$, $Q(q + 2q_s)$, with $q \approx -q_s$), which have almost degenerate frequencies.

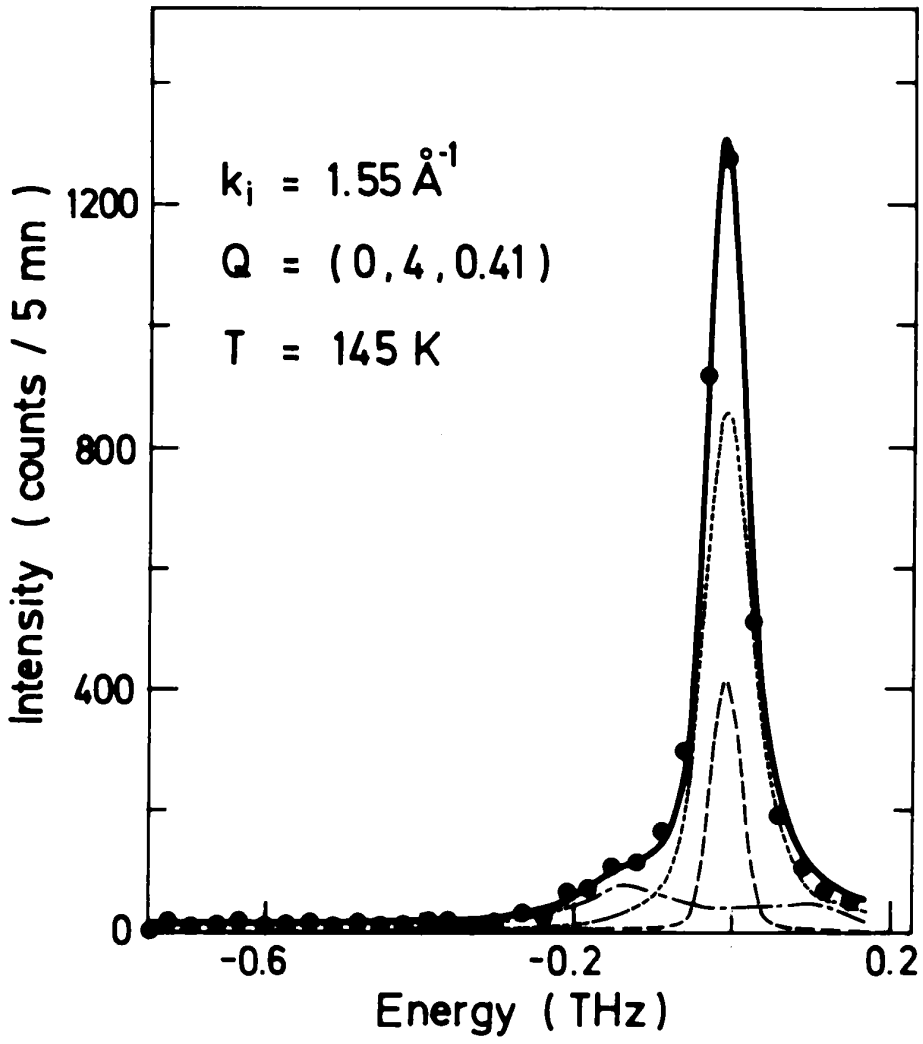

Figure 5. The experimental spectrum obtained for $\boldsymbol{Q} = (0\ 4\ 0.41)$ ($q = 0.41c^*$) at 145 K.

Both of the above assumptions are fulfilled in the extreme $T \rightarrow T_i$ limit, but we found that in the experimental situation corresponding to BCCD at 145 K only the first assumption can be retained.

Indeed, the first condition is fulfilled whenever there are only quartic terms in the anharmonic part of the potential and the modulation can be taken as sinusoidal. The case when the cubic term is present was studied in [31]. The cubic term leads to the appearance of even harmonics in the modulation and coupling between modes at q and $q \pm q_s$. However in BCCD, no cubic terms constructed from the coordinate of Λ_3–Λ_2 branches are allowed by symmetry. Also, no even harmonics of the modulation have been observed in the incommensurate phase of BCCD so far. We have thus kept only the anharmonic terms

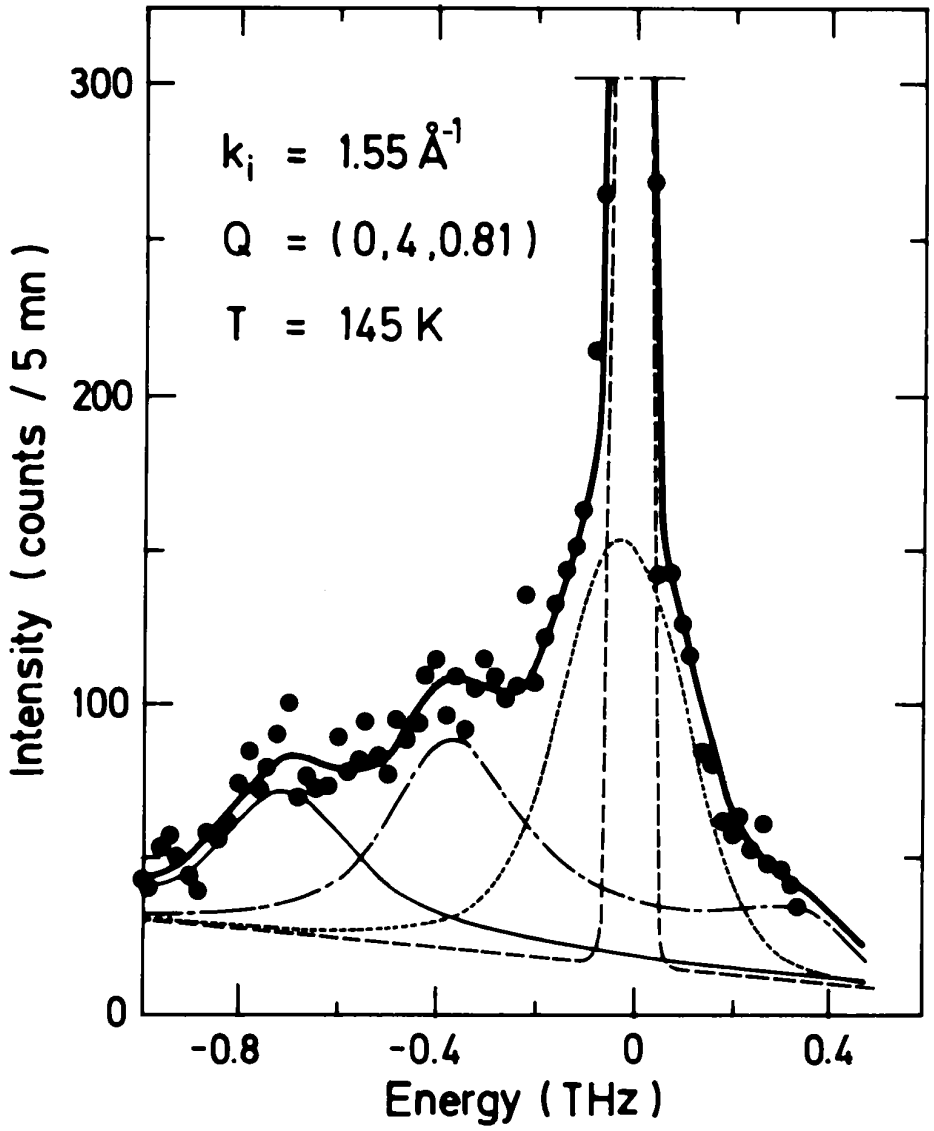

Figure 6. Phason, amplitudon and second optic branch at the (extended zone) wavevector ($q = 0.85c^*$), as measured at $\boldsymbol{Q} = (0\ 4\ 0.85)$, 20 K below T_i.

of lowest order in the soft-branch phonon coordinates—the quartic terms. Further, as the third-order satellites are quite small in BCCD at 145 K, only $\pm 2q_s$ couplings are considered in the following.

On the other hand, the second, more restrictive assumption, according to which the mode $Q(q)$ with $q \approx q_s$ is effectively mixed only with $Q(q - 2q_s)$, is quite important. It enables one to replace the infinite mode coupling matrix by a truncated 2×2 approximant. This procedure is justified if the coupling between $Q(q)$ and $Q(q + 2q_s)$ for $q \approx q_s$ is

much smaller than the difference $|\omega(q)^2 - \omega(q + 2q_s)^2|$. This is rather well fulfilled in crystals with strong dispersion. However, when the overall temperature renormalization of the soft branch $|\omega(T)^2 - \omega(T_i)^2|$ becomes comparable with $\omega(3q_s)^2$, the $Q(q) - Q(q + 2q_s)$ coupling can no longer be neglected [32]. For a crystal with weak soft-branch dispersion, as e.g. in the case of BCCD, this happens already quite close to $T = T_i$. We suggest an alternative coupling approximation. Unlike in the usual scheme, couplings of a $Q(q)$ mode to both $Q(q - 2q_s)$ and $Q(q + 2q_s)$ modes are fully taken into account. The coupling of the $Q(q + 2q_s)$ mode to the $Q(q + 4q_s)$ one is replaced by coupling to the $Q(q - 2q_s)$ mode. This last approximation is believed to be rather acceptable for q_s equal to roughly one-third of the wavevector at the Brillouin zone edge, because then one has $\omega(q+4q_s) \approx \omega(q-2q_s)$.

It can be verified [32] that, in the $T \to T_i$ limit, such an approximation scheme provides amplitudon and phason excitations with the same dispersion, eigenvectors and temperature dependence as the classical approach. One of the main advantages of this extended approach is that its application is not limited to the excitations derived from $Q(q)$ with $q \approx q_s$. The present *ansatz* is equally well justified at any point of the Brillouin zone.

Finally, for modelling of the real experimental situation in BCCD, it is necessary to include coupling terms to three other low-frequency branches [8]. Therefore, in order to estimate what changes should appear below T_i in the phonon spectra at a given wavevector q we have diagonalized the following 12×12 matrix:

$$\mathcal{M}_q = \begin{pmatrix} \mathcal{B}_{q-2q_s} + r\mathcal{A} & \Delta\mathcal{A} & \Delta\mathcal{A} \\ \Delta\mathcal{A} & \mathcal{B}_q + r\mathcal{A} & \Delta\mathcal{A} \\ \Delta\mathcal{A} & \Delta\mathcal{A} & \mathcal{B}_{q+2q_a} + r\mathcal{A} \end{pmatrix} \qquad \mathcal{A} = \begin{pmatrix} 0 & 0 & 0 & 0 \\ 0 & 0 & 0 & 0 \\ 0 & 0 & 1 & 0 \\ 0 & 0 & 0 & 1 \end{pmatrix}. \tag{6}$$

Here $\mathcal{B}_q$ is the 4×4 dynamical matrix describing the dispersion of the four lowest extended Λ_3–Λ_2 branches at T_i. This matrix is written in the form introduced in [8]:

$$\mathcal{B}_q = \begin{pmatrix} D_{vv} & 0 & D_{v\phi} & D_{v\psi} \\ 0 & D_{uu} & D_{u\phi} & D_{u\psi} \\ D^*_{v\phi} & D_{u\phi} & D_{\phi\phi} & D_{\phi\psi} \\ D_{v\psi} & D^*_{u\phi} & D^*_{\phi\psi} & D_{\psi\psi} \end{pmatrix} \tag{7}$$

where

$$\begin{aligned} D_{vv} &= A_a + A_c \sin^2(\pi q/2) \\ D_{uu} &= A_c \sin^2(\pi q/2) \\ D_{\phi\phi} &= b_{B_{2u}} + \left(b_{B_{1g}} - b_{B_{2u}}\right) \sin^2(\pi q/2) \\ D_{\psi\psi} &= b_{A_u} + \left(b_{B_{3g}} - b_{A_u}\right) \cos^2(\pi q/2) \end{aligned} \tag{8}$$

correspond to the dispersion of the bare translational optic branch, the bare transverse acoustic branch and the two symmetry related soft optic branches, respectively. The off-diagonal elements

$$\begin{aligned} D_{v\phi} &= \mathrm{i}d_c \sin \pi q \\ D_{v\psi} &= d_{B_{3g}} + d_{B_{1g}} \sin^2(\pi q/2) \\ D_{u\phi} &= d_{B_{1g}} \sin^2(\pi q/2) \\ D_{u\psi} &= \mathrm{i}d_c \sin \pi q \\ D_{\phi\psi} &= \mathrm{i}d_{12} \sin \pi q \end{aligned} \tag{9}$$

describe the dispersion of their mutual coupling constants. Note that the coupling and renormalization of the N-phase modes is the same for both soft optic branches and

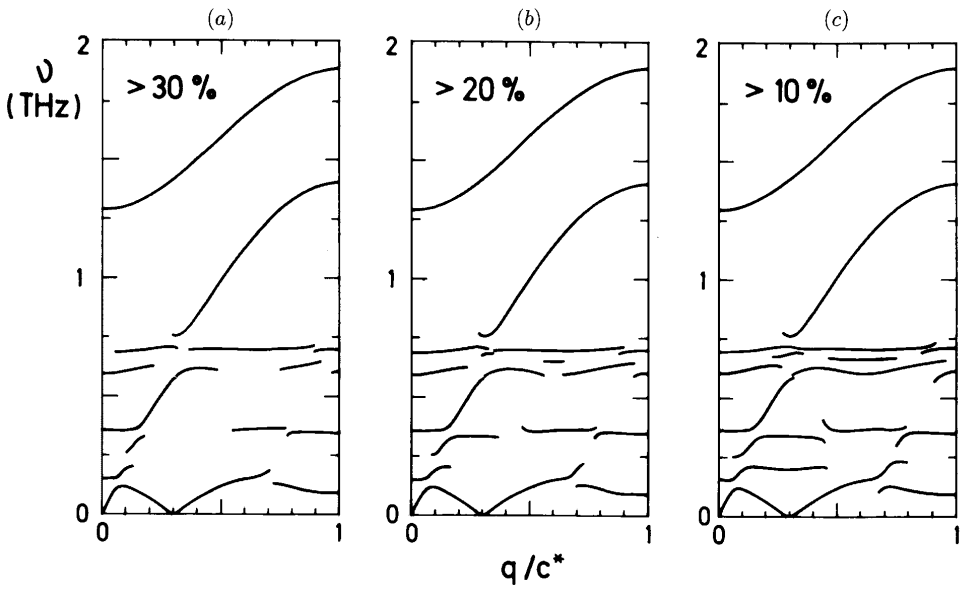

Figure 7. The frequency spectrum of the phonon excitations in the incommensurate phase of BCCD at 145 K: numerical results for the excitations derived from the four lowest Λ_3–Λ_2 branches of the parent N-phase, obtained from the effective three-oscillator approximation described in the text. Full lines are square roots of the eigenvalues of matrix (6), for which the factor (10) is larger than (*a*) 30%, (*b*) 20% and (*c*) 10%.

independent of the wavevector q (see (6)). This assumption reflects the experimental fact that both soft optic branches have rather uniform and similar temperature variation when plotted on an ω^2 scale [8].

The matrix $\mathcal{B}_q$ is parametrized by ten parameters, which were adjusted to the experimentally determined dispersions at $T = T_i$. Two additional parameters r and Δ describing the renormalization and mixing due to the static sinusoidal modulation were set to $r = 0.050$ and $\Delta = 0.068$. The value of the first parameter, which increases the frequency of the two bare optic modes, was chosen in order to achieve roughly the same degree of overall frequency renormalization as observed in the experiment at 145 K, while the parameter Δ was determined from the zero-frequency phason condition $\omega_{phason}(q_a) = 0$ solved numerically. The value of q_s was set to $0.306c^*$.

The eigenvalues ω_i^2 and the corresponding normalized eigenvectors $(\beta_{i;j})_{j=1,\ldots 12}$ of the $\mathcal{M}_q$ matrix (6) were then calculated numerically at each value of q. In order to select the excitations that are expected to contribute to a scattering process with momentum transfer $\boldsymbol{Q} = \boldsymbol{G} + \boldsymbol{q}$, we have evaluated for each mode i the factor

$$h_i = \sum_{j=5}^{7} |\beta_{i;j}|^2 \tag{10}$$

which describes the relative weight of the N-phase modes with wavevector q admixed in each given excitation ω_i. The frequencies of the excitations for which the factor (10) was higher than 10% are shown in figure 7.

5. Discussion and conclusion

The present experimental results show clearly that the excitation spectrum of BCCD at 145 K loses the character predicted by the usual approach derived in the $T \to T_i$ limit. The most remarkable difference is that the amplitudon–phason splitting of the soft-mode branch extends along the direction of modulation over the entire extended Brillouin zone.

The calculation dispersions obtained from the more general approach discussed in the preceding section are given in figure 7 and can be compared with the experimental dispersions in figure 1.

In general the agreement is quite satisfactory. The main difference is that while the experimental data were interpreted as due to the anticrossing of the transverse acoustic branch with only three continuous bare optic branches (phason branch, amplitudon branch and the branch near 0.6 THz), in the calculated dispersions all optic branches are further split into more components. These additional components are however of quite low intensity or their frequencies are separated by differences small with respect to typical damping parameter values, so they can hardly be resolved experimentally.

The present experimental results on BCCD at 145 K can be interpreted within a simple mode mixing model, in which the weak dispersion of the soft branch and the coupling of this branch to other branches in the same representation are taken into account.

Acknowledgment

We are indebted to T Janssen and V Dvořák for valuable comments on the theoretical part of the work and to Ph Boutrouille for help with various technical problems. During the final series of measurements we appreciated the assistance of two enthusiastic students, X Gagnard and L Buiron.

References

[1] Cummins H 1990 *Phys. Rep.* **185** 211
[2] Schaack G 1990 *Ferroelectrics* **104** 1477
[3] Dvořák V 1990 *Ferroelectrics* **104** 135
[4] Brill W, Schildkamp W and Spilker J 1985 *Z. Kristallogr.* **172** 281
[5] Zuniga F J, Expeleta J M, Pérez-Mato J M and Paciorek W 1991 *Phase Transitions* **31** 29
[6] Currat R, Legrand J F, Kamba S, Petzelt J, Dvořák V and Albers J 1990 *Solid State Commun.* **75** 545
[7] Hlinka J, Quilichini M, Currat R and Legrand J F 1996 *J. Phys.: Condens. Matter* **8** 8207
[8] Hlinka J, Quilichini M, Currat R and Legrand J F 1996 *J. Phys.: Condens. Matter* **8** 8221
[9] Cailleau H, Moussa F, Zeyen C M E and Bouillot J 1981 *J. Physique Coll.* **41** C6 704
[10] Quilichini M and Currat R 1983 *Solid State Commun.* **48** 1011
[11] Bernard L, Currat R, Delamoye P, Zeyen C M E, Hubert S and de Kouchkovsky R 1983 *J. Phys. C: Solid State Phys.* **16** 433
[12] Blinc E and Levanyuk A P (ed) 1986 *Incommensurate Phases in Dielectrics* (Amsterdam: Elsevier)
[13] Etrillard J, Toudic B and Bourges P private communication
[14] Axe J D 1976 *Proc. Gatlinburg Neutron Scattering Conf.* CONF-760601-P1
[15] Volkov A A, Goncharov Yu G, Kozlov G V, Albers J and Petzelt J 1986 *JETP Lett.* **44** 603
[16] Ao R and Schaack G 1988 *Indian J. Pure Appl. Phys.* **26** 124
[17] Wilhem H and Unruh H G 1991 *Z. Kristallogr.* **95** 75
[18] Kamba S, Dvořák V, Petzelt J, Goncharov Yu G, Volkov A A and Kozlov G V 1993 *J. Phys. Condens. Matter* **5** 4401
[19] Kamba S, Petzelt J, Železný V, Smutný F, Dvořák V, Hlinka J, Quilichini M, Volkov A A, Gorschunov B P, Kozlov G V, Currat R and Legrand J F 1994 *Ferroelectrics* **159** 97

[20] Hennion B, system of programs for the correction of inelastic neutron spectra for triple-axis resolution effects, available at LLB, CE Saclay
[21] Bruce A D and Cowley R A 1978 *J. Phys. C: Solid State Phys.* **11** 3609
[22] Dvořák V 1980 *Karpacz Winter School 1979 (Lecture Notes in Physics)* (Springer)
[23] Zeyher R and Finger W 1982 *Phys. Rev. Lett.* **49** 1833
[24] Quilichini M, Pasquier B, LeCalvé N, Hlinka J, Gagnard X and Buiron L unpublished Raman data on fully deuterated BCCD
[25] Garcia A, Pérez-Mato J M and Madariaga G 1989 *Phys. Rev.* B **39** 2476
[26] Overhauser A W 1971 *Phys. Rev.* B **3** 3173
[27] Axe J D 1980 *Phys. Rev.* B **21** 4181
[28] Adlhardt W 1982 *Acta Crystallogr.* A **38** 498
[29] Pérez-Mato J M, Madariaga G and Elcoro L 1991 *Solid State Commun.* **1** 33
[30] Currat R and Janssen T 1988 *Solid State Phys.* **41** 201
[31] Walker M B 1978 *Can. J. Phys.* **56** 127
[32] Hlinka J 1992 *PhD Thesis* Université d'Orsay